CHAPTER IV
EFFECT OF Ti, Zr, Hf AND V ON HYDROGEN DESORPTION/ ABSORPTION OF $NaAlH_4$

4.1 Abstract

The main objective of this work was to investigate the effects of transition metals ($TiCl_3$, $ZrCl_4$, $HfCl_4$, and VCl_3) on the hydrogen desorption/absorption of $NaAlH_4$. The samples were prepared by milling $NaAlH_4$ with each transition metal at 300 rpm for 20 min. The hydrogen desorption was carried out over a wide temperature range from room temperature to 280°C while the hydrogen re-absorption took place at 120°C under hydrogen pressure of 11 MPa. The result reveals that in the first cycle, the desorption temperature of metal doped $NaAlH_4$ is lowered to 90°C, almost half of the temperature of the undoped $NaAlH_4$ (196°C). The complete hydrogen desorption of undoped $NaAlH_4$ releases about 5.1 wt% (H/M) while the amount of released hydrogen of the ones doped with each of the transition metals is lower, 4.5 wt% (H/M), because of the partial decomposition during the milling process. In the subsequent cycles, hydrogen can be re-absorbed in the doped $NaAlH_4$ samples about 30-75% of their original hydrogen capacity. $TiCl_3$ doped $NaAlH_4$ shows the highest reversible hydrogen capacity up to 3.85 wt% (H/M) and the rate of hydrogen re-absorption. XRD analysis demonstrates that after subsequent desorption/absorption, there is an evidence of Al-V alloy in the VCl_3 doped sample and Al-Hf alloy in the $HfCl_4$ doped sample, but no Ti-compound is observed for the $TiCl_3$ doped sample.

4.2 Introduction

Sodium aluminiumhydride or sodium alanate, $NaAlH_4$, has been considered as a candidate media for on-board hydrogen storage in fuel cell applications, in part, because of their high hydrogen content. $NaAlH_4$ decomposes into two steps, as shown in Eqs. (4.1) and (4.2). The first step releases 3.7 wt% hydrogen at 185°C and

the second one at 250°C with 1.8 wt% hydrogen [1-2].

$$3NaAlH_4 \rightarrow Na_3AlH_6 + 2Al + 3H_2, \quad (4.1)$$

$$Na_3AlH_6 \rightarrow 3NaH + Al + \frac{3}{2}H_2 \quad (4.2)$$

The material has become even more attractive, thanks to the results from Bogdanovic and Schwickardi [3]. It was reported that $NaAlH_4$, mixed with $Ti(OBu^n)_4$, can desorb 3.5 – 4 wt% hydrogen and reabsorb hydrogen at 170°C and 150 bar. After this breakthrough, attempts have been made to develop and modify hydrogen desorption/absorption in terms of its kinetics, capacity and reversibility of alkali-metal aluminohydrides [4-9].

However, none has met the U.S. Department of Energy goals (6.0 wt% hydrogen for 2010) [10]. An understanding of the hydrogen desorption/absorption of $NaAlH_4$ doped with transition metal is still unclear. The questions are: How do metal dopants activate the hydrogen desorption/re-absorption in $NaAlH_4$?; What is the state of metal species after doping?; and Why does Ti dopant show higher potential than other metal dopants in the hydrogen desorption/re-absorption in $NaAlH_4$?. There are a number of proposed mechanisms, one of which suggested that Ti dopant might catalyze the hydrogen desorption/absorption of $NaAlH_4$. The substitution of dopant in the lattice of $NaAlH_4$ affects the activation and involves the lattice distortions as proposed by Sun *et al.* [11]. In the mechanism, Ti is thought to substitute Na^+ and form Ti^{4+} with $Ti(OBu^n)_4$ doped less than 2 mol% resulting in lattice distortions and vacancy formation and enhancement of hydrogen desorption kinetics. However, the proposed mechanisms by Graetz *et al.* using Ti K-edge x-ray absorption near-edge spectroscopy shows that Ti does not substitute in the bulk lattice nor form Ti metal, but it is present on the surface in the form of amorphous $TiAl_3$ [12-13].

The purpose of this work was then to present the effects of a transition metal ($TiCl_3$, $ZrCl_4$, $HfCl_4$, and VCl_3) on the hydrogen desorption/re-absorption of $NaAlH_4$ and to understand how each dopant acts in the hydride.

4.3 Experimental

4.3.1 Materials

$NaAlH_4$ (90% purity), $ZrCl_4$ (> 99.9% purity), $HfCl_4$ (98% purity) were purchased from Aldrich Chemical. VCl_3 (99% purity) was purchased from Merck. $TiCl_3$ (Riedel-de Haën) was obtained from vacuum drying of 12% $TiCl_3$ in hydrochloric acid (see detail of preparation in Chapter 3).

4.3.2 Hydrogen desorption/absorption

All experiments in this study were performed under dry nitrogen atmosphere. The as-received $NaAlH_4$ sample was doped with $TiCl_3$, $ZrCl_4$, $HfCl_4$, and VCl_3 using a centrifugal ball mill (Retsch ball mill model S100, stainless steel vial size 250 ml, stainless balls with 1 cm and 2 cm diameters) for 20 min with a speed of 300 rpm. Immediately after mixing, approximately 1 g of a sample was placed into the thermovolumetric apparatus. The high pressure stainless steel reactor (316SS) was heated from room temperature to 280°C via a furnace controlled by a PID temperature controller. The K-type thermocouple was placed inside the reactor to measure the temperature. The pressure transducer (Cole Parmer, model 68073-68074) was used to measure the pressure change resulting from hydrogen desorption from the sample. For the absorption experiments, hydrogen (99.9995%) was used to pressurize the high pressure vessel in a step-wise manner. The sample was re-absorbed at about 120°C and 10 MPa overnight. Once the pressure reading was constant over a period of time, the data was used to calculate the amount of hydrogen absorbed on the sample. Amount of the released hydrogen shown in the results (H/M) was calculated with respect to the amount of $NaAlH_4$ in the sample. The same procedure was repeated to investigate their reversibility. A schematic diagram of the experimental set-up is shown in Figure 4.1.

Sample characterization was also performed using a Rigaku x-ray diffractometer at room temperature over a range of diffraction angles from 28-80 with CuK-alpha radiation (40 kV, 30 mA) in order to understand the phase transformation and the roles of the transition metals on the hydrides.

4.4 Results and Discussion

4.4.1 Hydrogen desorption/absorption on doped $NaAlH_4$

Figure 4.2 shows the temperature program desorption in the first cycle of milled $NaAlH_4$, $NaAlH_4$ doped with 4 mol% $HfCl_4$ (4%$HfCl_4$-$NaAlH_4$), $NaAlH_4$ doped with 4 mol% $TiCl_3$ (4%$TiCl_3$-$NaAlH_4$), $NaAlH_4$ doped with 4 mol% $ZrCl_4$ (4%$ZrCl_4$-$NaAlH_4$), and $NaAlH_4$ doped with 4 mol% VCl_3 (4%VCl_3-$NaAlH_4$). The decomposition of undoped $NaAlH_4$ takes place at the temperature of 196 – 260°C with the released hydrogen ~ 5.1 wt% (H/M) while $NaAlH_4$ doped with metals decomposes hydrogen at lower temperature compared to undoped $NaAlH_4$. 4%$ZrCl_4$-$NaAlH_4$ and 4%$TiCl_3$-$NaAlH_4$ seem to show the lowest desorption temperature at 103°C followed by the ones doped with $HfCl_4$ at 121°C and VCl_3 at 135°C. It is clearly observed that $NaAlH_4$ doped with different metals behaves differently during the two-step hydrogen desorption. The 1st desorption step of metal doped $NaAlH_4$ occurs at the temperature range of 103 – 185°C, while the 2nd desorption step starts at the temperature about 200°C. The total amount of released hydrogen in the 1st cycle of 4%$TiCl_3$-$NaAlH_4$, 4%$ZrCl_4$-$NaAlH_4$, and 4%VCl_3-$NaAlH_4$ are around 4.5 wt% (H/M), which is lower than that of undeopd $NaAlH_4$. This is because some $NaAlH_4$ decomposes during the milling process. This suggests that doping one of the metals can accelerate the decomposition between Al-H bonds and decrease the decomposition temperature of $NaAlH_4$. Moreover, the milling process also assists in the acceleration of the decomposition of $NaAlH_4$.

Figure 4.3 shows temperature program desorption of 4%VCl_3-$NaAlH_4$ prepared by centrifugal ball milling in different media (stainless steel balls and vial compared with a 250-ml agate vial and 5 of 1-cm-diameter and 2 of 2-cm-diameter agate balls). We found that the sample milled by the stainless ball mill possesses 35°C lower desorption temperature than the one milled by the agate ball mill. This may be due to the different types of ball mill resulting in different particle sizes, different microstain, and homogeneity of the samples. However, the hydrogen desorption from both milling media are only slightly different, as indicated by the slopes.

After the 1st desorption, the sample was subsequently re-absorbed under 11 MPa of hydrogen pressure at 120°C for 10-12 h. Figures 4.4 -4.7 show the reversibility of the hydrogen desorption/re-absorption of $NaAlH_4$ doped with different metals. It was found that all tested metals contribute to the reversibility of $NaAlH_4$. About 30-75% of their original hydrogen capacity can be re-absorbed in the samples. $NaAlH_4$ doped with $TiCl_3$ exhibits the highest reversible hydrogen capacity. It can re-absorb hydrogen up to 3.85 wt% (H/M) while the reversible hydrogen capacity of $HfCl_4$-$NaAlH_4$, $ZrCl_4$-$NaAlH_4$, and VCl_3-$NaAlH_4$ are about 2.75 wt% (H/M), 2.5 wt% (H/M), and 1.5 wt% (H/M), respectively. In addition, it can be observed that the desorption temperature in the subsequent cycle shifted to the higher ones compared with the first desorption. This may be suggested that, after the first desorption, the sample particles melt due to the high temperature (higher than the melting point of $NaAlH_4$, 178°C) resulting in the segregation of particles, especially Al particles [2].

Figure 4.8 shows the hydrogen re-absorption rate in the third cycle of $NaAlH_4$ doped with different metal catalysts by plotting between time and pressure at the initial state and final state of the absorption. It reveals that $TiCl_3$ is the best catalyst in both re-absorption rate and hydrogen capacity, followed by Zr, Hf and V.

This study substantiates that the transition metals improve the hydrogen desorption/re-absorption of $NaAlH_4$ and decrease the temperature of desorption compared with undoped $NaAlH_4$. To understand the role of transition metal on the hydrogen desorption/re-absorption of $NaAlH_4$, the samples were characterized by the XRD technique.

4.4.2 X-ray diffraction

After hydrogen desorption/absorption, the samples were characterized by the Rigaku x-ray diffractometer. Due to the air sensitivity of the samples, they were covered with a Kapton tape layer to minimize any contamination. Figure 4.9 shows XRD patterns of undoped $NaAlH_4$ milled by (a) stainless balls/vial and (b) agate balls/vial. The X-ray pattern of the sample milled by the stainless steel vial/balls is broader than that of the sample milled by the agate vial/balls. This result indicates that the higher energy of milling leads to the lower crystallinity of $NaAlH_4$.

Thus, the distorted crystalline of $NaAlH_4$ may destabilize the bond between Al and H, which would consequently cause the lowering in the desorption temperature of the milled $NaAlH_4$ sample as previously discussed.

Illustrated in Figure 4.10 is the comparison of XRD patterns of the undoped $NaAlH_4$ sample after the hydrogen desorption at different conditions: the sample after milling (a); the desorbed sample at 220°C (b), and 280°C (c). In the first desorption step at ~ 220°C, Na_3AlH_6 and Al were observed along with $NaAlH_4$ in the sample. Progressive hydrogen desorption at 280°C to complete the desorption resulted in the total conversion of the hydride to NaH and Al. Furthermore, the increase in the intensity and narrow peak of aluminum shows the formation of aluminum crystallites. This result is in good agreement with the results of Meisner *et al.* [14].

Figure 4.11 shows the XRD patterns of all fresh $NaAlH_4$ samples doped with metals compared with undoped $NaAlH_4$ after milling, peaks of Al can be obviously observed after the milling for all $NaAlH_4$ samples doped with metals. In addition, the broaden peak of NaCl appears for the sample doped with $ZrCl_4$. This result indicates that there may be a reaction between $NaAlH_4$ and metal chloride to form as NaCl, which can be written as follow:

$$xNaAlH_4 + MCl_x \rightarrow xNaCl + M + x[AlH_4]^- \rightarrow xNaCl + M + xAl^0 + 2xH_2. \qquad (4.3)$$

This result confirms that the distortion of some $NaAlH_4$ by metal doping also leads to the partial decomposition of the doped hydride during the milling process. Thus, the reason why metal doping can reduce the hydrogen desorption temperature of $NaAlH_4$ is because the reaction between $NaAlH_4$ with a metal chloride forms NaCl and the $[AlH_4]^-$ anion but this hydride is unstable so it can easily decompose to Al and H_2.

After complete desorption, XRD results show the increase in the formation of NaCl and Al including NaH for all samples as shown in Figure 4.12 while the main constituents consist of $NaAlH_4$, Al, and NaCl for the all re-absorbed samples (Figure 4.13), in addition to the presence of Na_3AlH_6 for the samples doped with $ZrCl_4$, $HfCl_4$, and VCl_3. This result indicates that the formation of non-reducible

species on the desorbed samples entails with the lowering in hydrogen re-absorption. In other words, the total reversibility of the desorbed samples could not be achieved to their original state due to the presence of Al, Na_3AlH_6, and NaCl (as observed for the samples after several desorption/absorption cycles). Lastly, we cannot observe any peaks of the transition metal compound in the samples after the hydrogen desorption/absorption by the XRD technique, except the sample doped with VCl_3. As shown in Figure 4.12(d) and Figure 4.13(d), some unknown peaks were clearly found at $2\theta \sim 41°$ in the sample doped with VCl_3. These peaks were expected to be the formation of V-species. Peak identification using JCPD-International Centre for Diffraction Data suggested that they should be peaks of an alloy compound of V-Al in the form of Al_3V. This supports the visibility of V-Al peaks in VCl_3 doped $NaAlH_4$. In the case of $TiCl_3$, $ZrCl_4$, or $HfCl_4$ doped $NaAlH_4$, no metal peak is observed by the XRD technique. It is possible that the metal in those samples is in the form of amorphous or amount of metal in the hydride samples is very dilute so the diffraction peak is difficult to be visible by the XRD.

To determine the location of the Hf-compound in the $NaAlH_4$ sample, 10 mol% $HfCl_4$ were doped in $NaAlH_4$, after the subsequent hydrogen desorption/absorption, the sample doped with 10 mol% $HfCl_4$ was dissolved in THF (>99.998%, J.T. Baker), stirred for 2 h and centrifuged in order to separate the precipitate. Finally, the precipitate was dried by vacuum and characterized by XRD. Surprisingly, the XRD pattern of the THF precipitated sample shows some unknown peaks at $2\theta \approx 41.5°$ and 50.48°, which match with the reference data base of compound between Hf-Al would be in form of Al_3Hf as shown in Figure 4.14(b). It is also the same with in case of $ZrCl_4$-$NaAlH_4$, i.e. the diffraction peak of Zr-Al is visible when the sample doped with > 10 mol% $ZrCl_4$ reported by Weidenthaler *et al.* [15]. In contrast with $TiCl_3$-$NaAlH_4$, the diffraction peak of Ti compound cannot be observed although the amount of $TiCl_3$ doping was increased. This may indicate that Ti forms as an amorphous compound in the hydride system. In addition, Graetz *et al.* [12] confirmed the present of Ti in the system using X-ray absorption, which reported that Ti is atomically dispersed in the hydride system in form of $TiAl_3$ amorphous alloy.

The result confirms that the doped metal in the $NaAlH_4$ system locates with Al in the form of alloy. So it can be suggested that the role of metal alloy is to involve as an active species in the dissociation of hydrogen. H atom then diffuses into the bulk of Al and forms as a hydride of aluminum or alane. From the literature, AlH_3 can react simultaneously with NaH to form Na_3AlH_6 and $NaAlH_4$, as reported by Chaudhuri *et al.* [16], Eqs. (4.4) and (4.5).

$$AlH_3 + 3NaH \rightarrow Na_3AlH_6 \tag{4.4}$$

$$Na_3AlH_6 + 2AlH_3 \rightarrow 3NaAlH_4. \tag{4.5}$$

Comparison the ability of each metal on the hydrogen re-absorption shows that Ti-$NaAlH_4$ possesses a higher ability to re-absorb hydrogen than Zr-, Hf- or V-$NaAlH_4$. The question is why Ti has more activity than Zr, Hf, and V on the hydrogen re-absorption of $NaAlH_4$. From the XRD results, there are differences of species in the Ti-$NaAlH_4$ system and the Zr-, Hf- or V-$NaAlH_4$ system. The formation of Al-Zr, Al-V, and Al-Hf in the hydride system is in form of crystalline while Ti forms as Ti-Al amorphous. It was reported that Ti-Al amorphous highly disperses on or in the hydride system. In other words, Ti-Al lacks a long-range order to form Ti-Al crystal structure because it prefers to be highly dispersed particles in the hydride system [12]. This property of Ti resulted in the highest activity to catalyze the hydrogen re-absorption of the desorbed sample. In contrast, the formation of alloy between Al with Zr, Hf, or V prefers a long-range order, this leads to the decrease in the dispersion of the active sites for hydrogen dissociation into the desorbed samples. Besides the activity of metal dopant, the aggregation and segregation among species in the desorbed sample, particularly for Al, also influence the hydrogen re-absorption, because the aggregation and segregation increase the distance pathway for hydrogen diffusion into the desorbed sample and cause the incomplete hydrogen re-absorption of the sample in the subsequent cycle as evidenced by the Na_3AlH_6 phases in the re-absorbed sample.

4.5 Conclusion

Doping transition metals ($TiCl_3$, $ZrCl_4$, $HfCl_4$, or VCl_3) on $NaAlH_4$ affects the hydrogen desorption/absorption. $TiCl_3$ seems to be the most effective dopant among the four tested transition metals. By doping $NaAlH_4$ with $TiCl_3$, the maximum hydrogen absorption capacity can be restored at 3.85 wt% (H/M). The role of metal on the reversible reaction of the desorbed hydride involves with catalyzing the hydrogen dissociation into Al bulk. The location of metal (Zr, Hf, and V) in the system is in the form of crystal alloy with Al, while Ti forms as Ti-Al amorphous, which disperses in the hydride system. This may promote more active sites for hydrogen dissociation in Ti doped-hydride. However, hydrogen cannot be completely re-absorbed in the desorbed hydrides. That is due to the segregation of Al phase, the formation of a by-product (NaCl), and consumed Al to form alloy with a metal catalyst.

4.6 Acknowledgements

This work was supported by the National Science and Technology Development Agency (Reverse Brain Drain Project); the Petroleum and Petrochemical College (PPC), the Research Unit for Petrochemical and Environment Catalysts, the Ratchadapisek Somphot Endowment, and National Center of Excellence for Petroleum, Petrochemicals and Advanced Materials, Chulalongkorn University; and UOP LLC.

4.7 References

[1] C.M. Jensen, K.J. Gross, Appl. Phys. A, 329 (2001) 213-219.

[2] B. Bogdanović, R.A. Brand, A. Marjanović, M. Schwickardi, J. Tölle, J. Alloys Compd., 302 (2000) 36-58.

[3] B. Bogdanović, M Schwickardi, J. Alloys Compd., 253 (1997) 1-9.

[4] A. Zidan, S. Takara, A. Hee, C.M. Jensen, J. Alloys Compd., 285 (1999) 119-122.

[5] M. Jensen, R. Zidan, N. Mariels, A. Hee, C. Hagen, Int. J. Hydrogen Energy, 24 (1999) 461-465.

[6] C.M. Jensen, S. Takara, Proceedings of the 2000 on Hydrogen Program Review NREL/CP-570-28890, (2000).

[7] K.J. Gross, E.H. Majzoub, S.W. Spangler, J. Alloys Compd., 356-357 (2003) 423-428.

[8] G. Sandrock, K. Gross, G. Thomas, J. Alloys Compd., 399 (2002) 299-308.

[9] D.L. Anton, J. Alloys Compd., 356-357 (2003) 400-404.

[10] D. Sun, S. Ma, Y. Ke, D.J. Collins, H.C. Zhou, J. Am. Chem. Soc., 128 (2006) 3896-3897.

[11] D. Sun, T. Kiyobayashi, H.T. Takeshita, N. Kuriyama, C.M. Jensen, J. Alloys Compd., 337 (2002) L8-L11.

[12] J. Graetz, J.J. Reilly, Johnson, J. App. Phy. Lett., 85 (2004) 500-503.

[13] H.W. Brink, C.M. Jensen, S.S. Srinivasan, B.C. Hauback, D. Blanchard, K. Murphy, J. Alloys Compd., 376 (2004) 215-221.

[14] G.P. Meisner, G.G. Tibbetts, F.E. Pinkerton, C.H. Olk, M.P. Balogh, J. Alloys Compd., 337(2002) 254-263.

[15] C. Weidenthaler, A. Pommerin , M. Felderhoff, B. Bogdanovic, F. Schüth, Phys. Chem Chem Phys., 5(2003) 5149-5153.

[16] S. Chaudhuri, J. Graetz, A. Ignatov, J. Reilly, J.T. Mucherman, J. Am. Chem. Soc., 128(2006) 11404-11415.

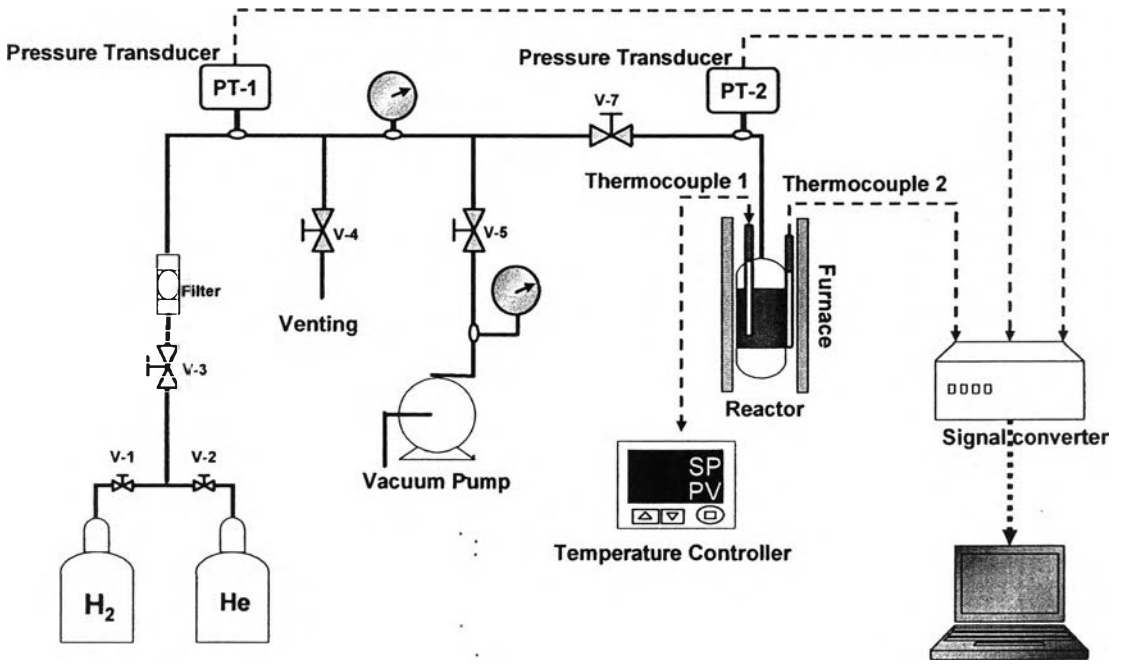

Figure 4.1 Schematic diagram of experimental set-up.

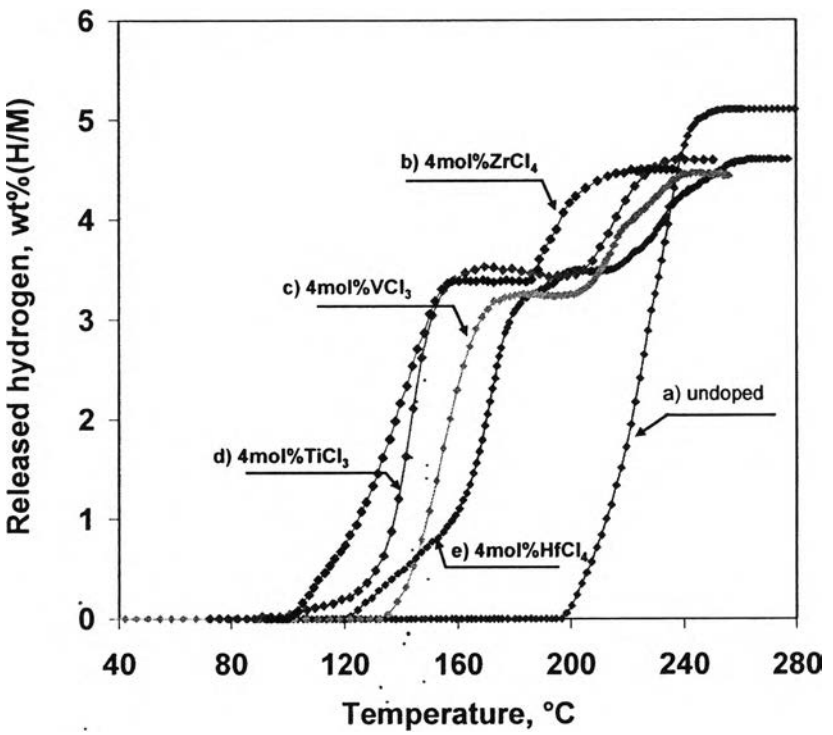

Figure 4.2 Correlation between temperature and hydrogen capacity, during the 1st hydrogen desorption on $NaAlH_4$: a) undoped $NaAlH_4$ b) 4%$ZrCl_4$- $NaAlH_4$ c) VCl_3-$NaAlH_4$, d) 4%$TiCl_3$-$NaAlH_4$, and e) 4%$HfCl_4$-$NaAlH_4$.

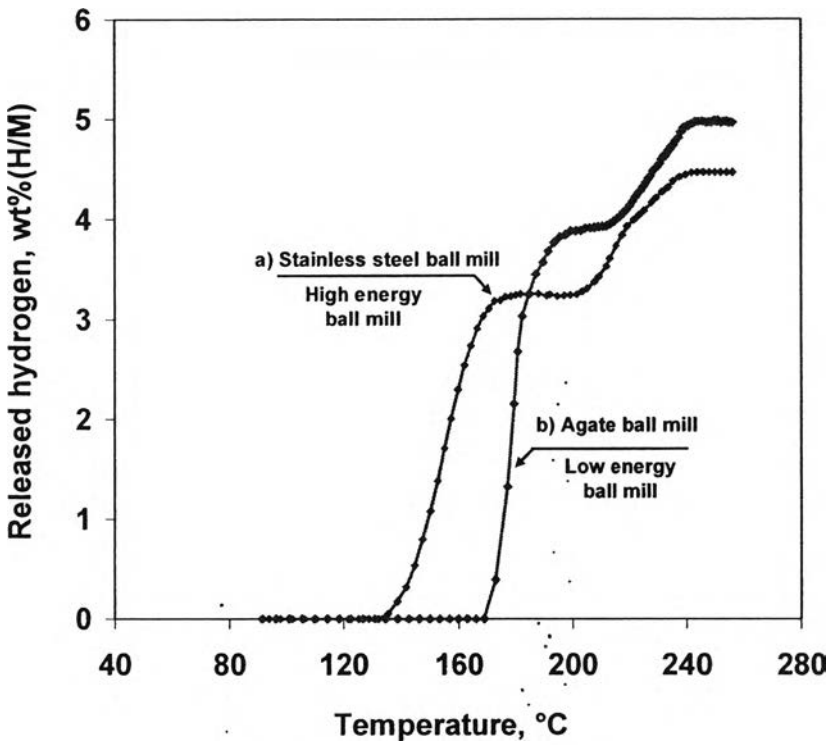

Figure 4.3 Correlation between temperature and hydrogen released during the 1st hydrogen desorption on $NaAlH_4$ doped 4 mol% VCl_3 by a) stainless steel ball milling, and b) agate ball milling for 20 min.

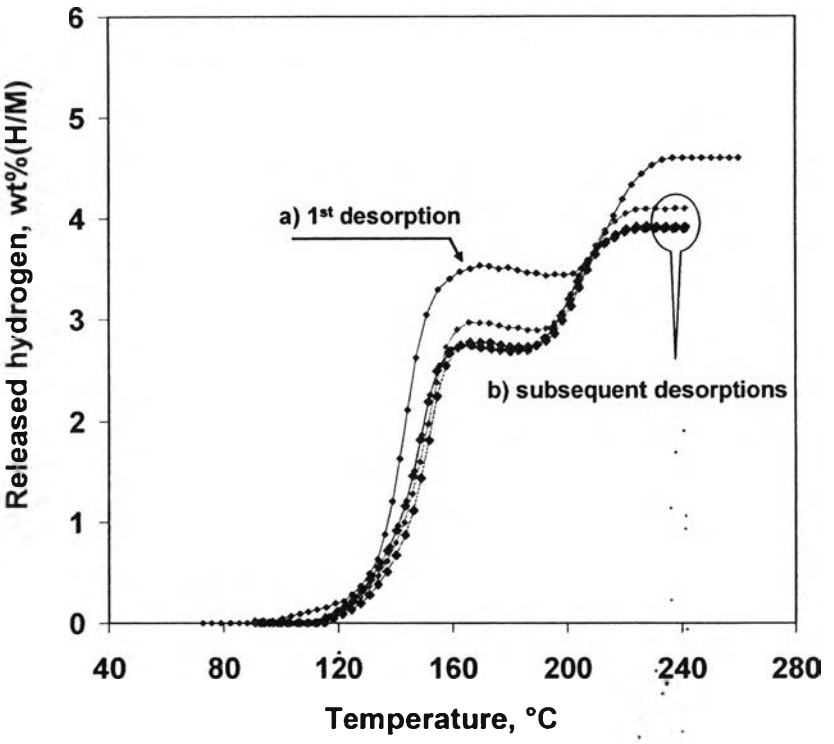

Figure 4.4 Correlation between temperature and hydrogen released during hydrogen desorption on $NaAlH_4$ doped with 4 mol% $TiCl_3$: a) first desorption and b) subsequent desorptions.

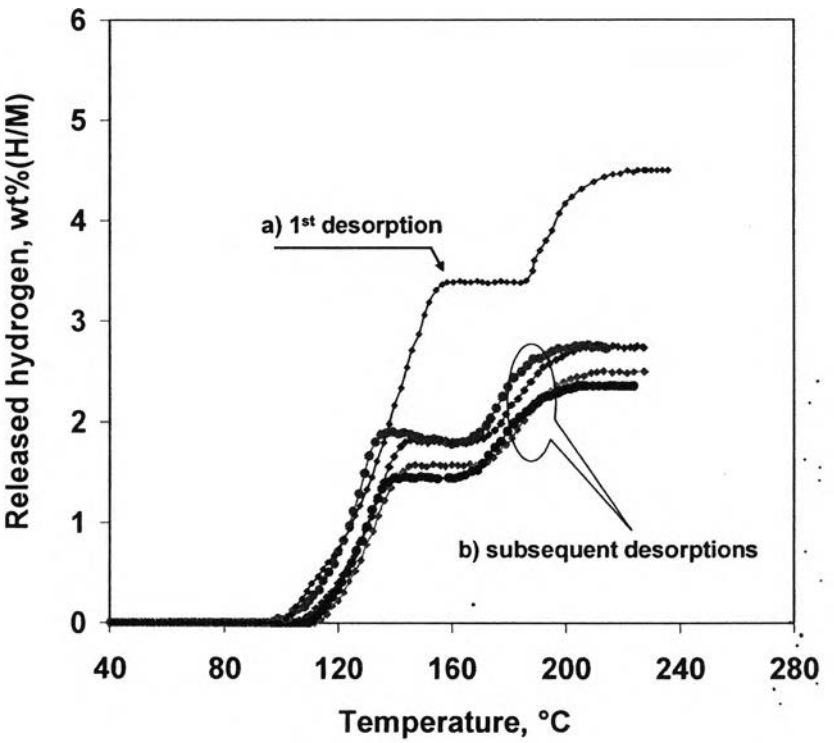

Figure 4.5 Correlation between temperature and hydrogen released during hydrogen desorption on $NaAlH_4$ doped with 4 mol% $ZrCl_4$: a) first desorption and b) subsequent desorptions.

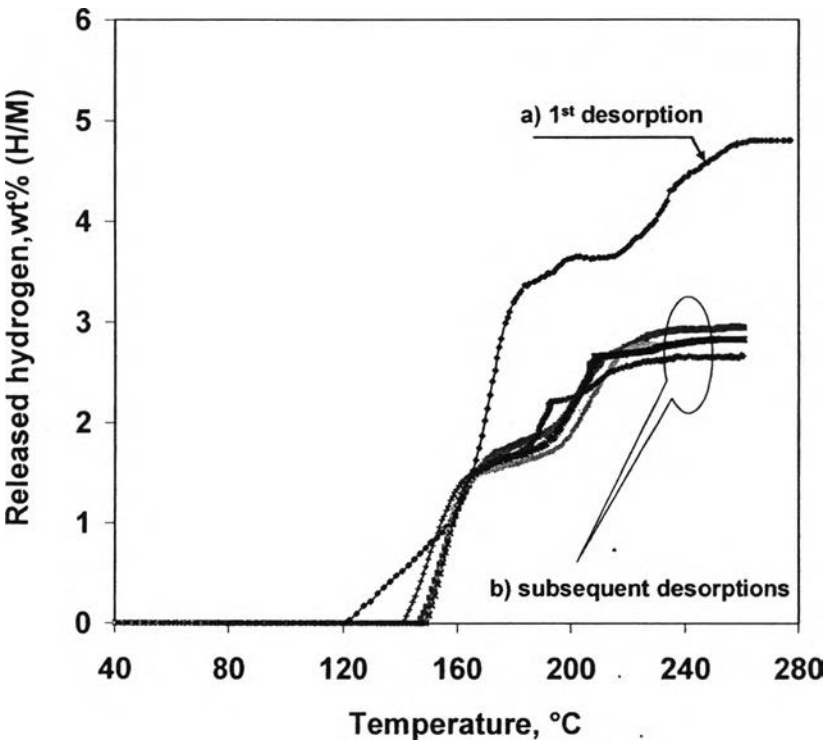

Figure 4.6 Correlation between temperature and hydrogen released during hydrogen desorption on $NaAlH_4$ doped with 4 mol% $HfCl_4$: a) first desorption and b) subsequent desorptions.

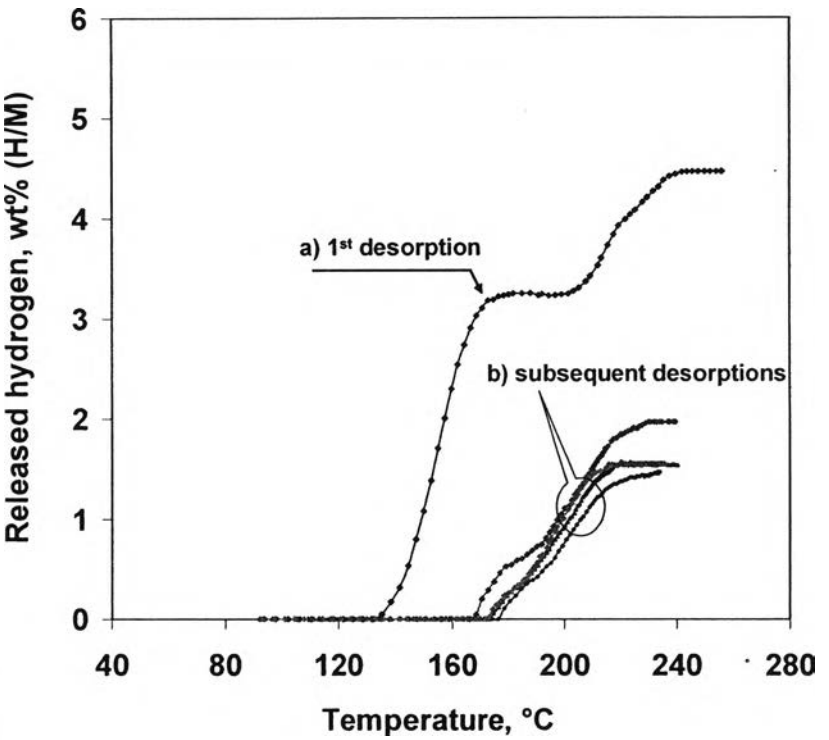

Figure 4.7 Correlation between temperature and hydrogen released during hydrogen desorption on $NaAlH_4$ doped with 4 mol% VCl_3: a) first desorption and b) subsequent desorptions.

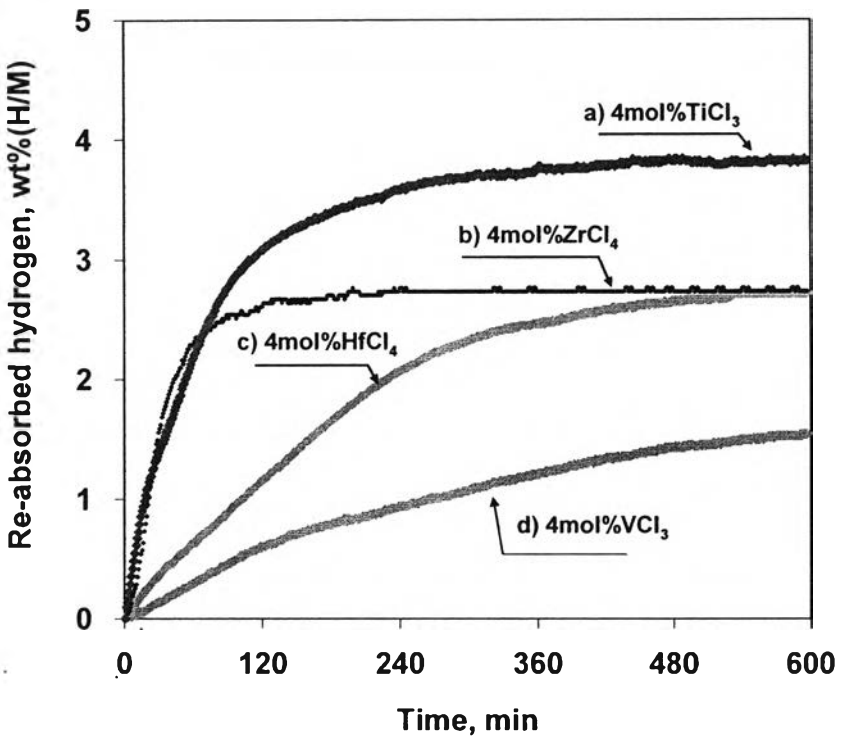

Figure 4.8 The hydrogen re-absorption rate in the 3rd cycle of a) 4%$TiCl_3$-$NaAlH_4$, b) 4%ZrCl4-NaAlH4, c) 4%$HfCl_4$-$NaAlH_4$, and d) VCl_3-$NaAlH_4$.

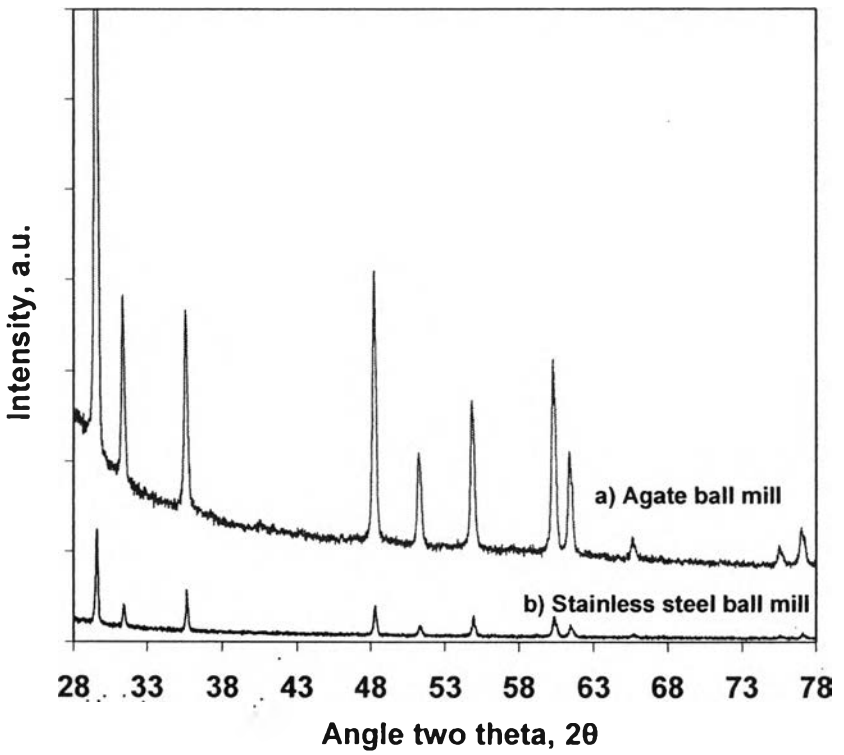

Figure 4.9 XRD patterns of milled $NaAlH_4$ by: a) agate ball milling and b) stainless steel ball milling.

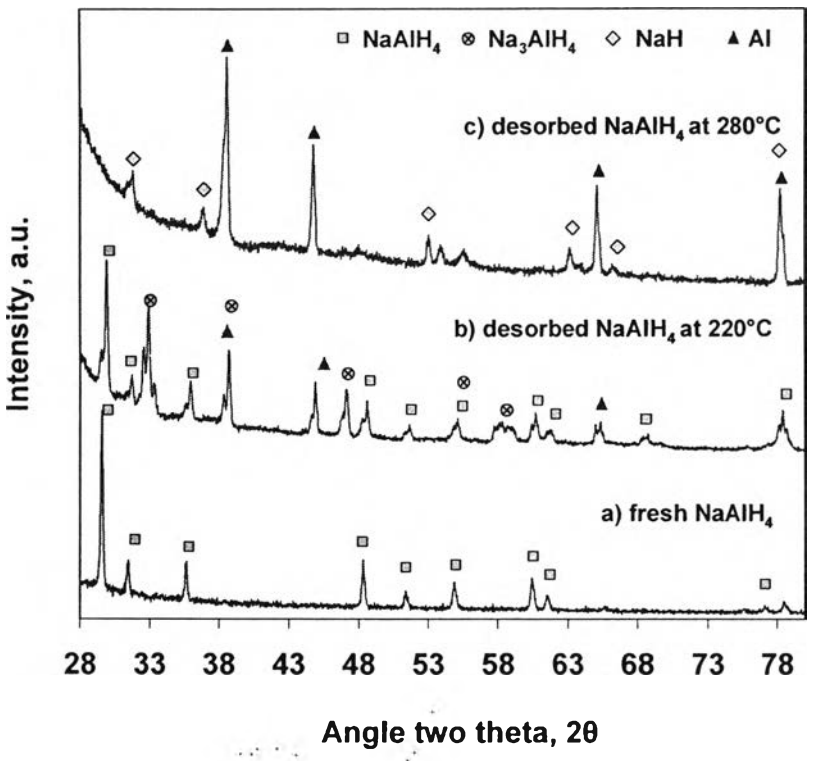

Figure 4.10 XRD patterns of a) fresh $NaAlH_4$ after milling, b) desorbed $NaAlH_4$ at 220°C, and c) desorbed $NaAlH_4$ at 280°C.

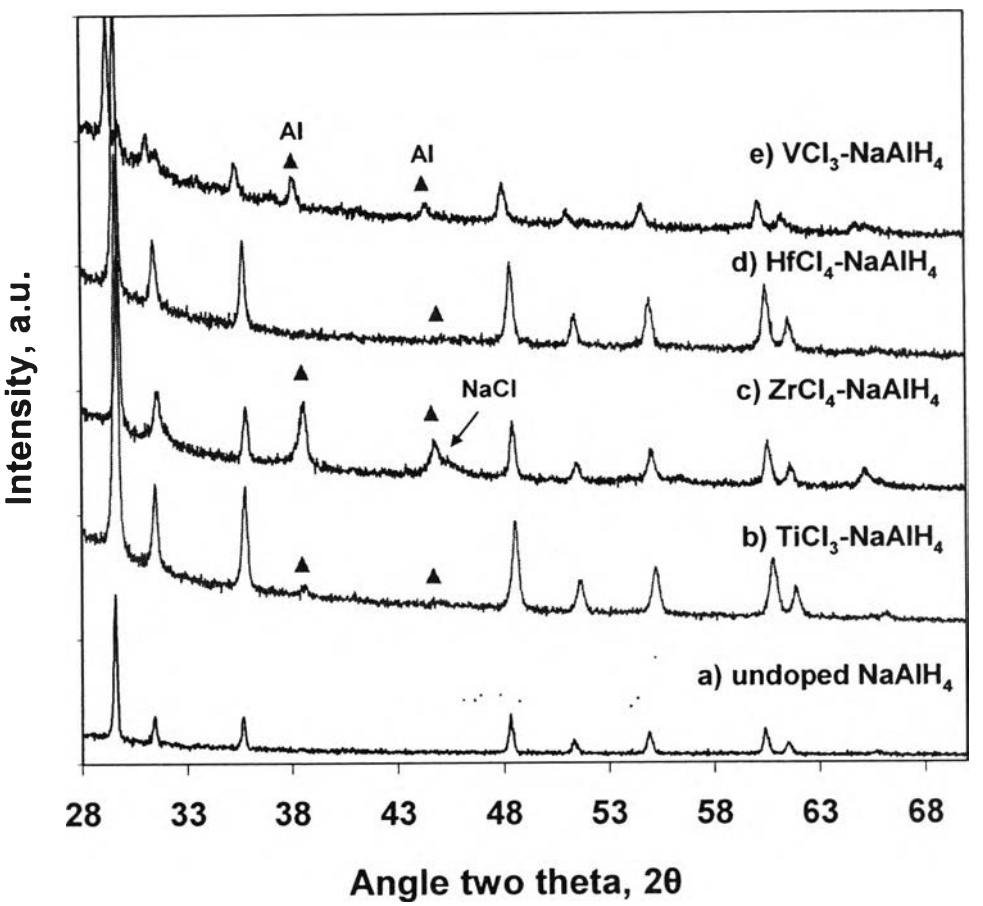

Figure 4.11 XRD patterns of a) undoped $NaAlH_4$, b) $TiCl_3$-$NaAlH_4$, c) $ZrCl_4$-$NaAlH_4$, d) $HfCl_4$-$NaAlH_4$, and e) VCl_3-$NaAlH_4$ after milling process.

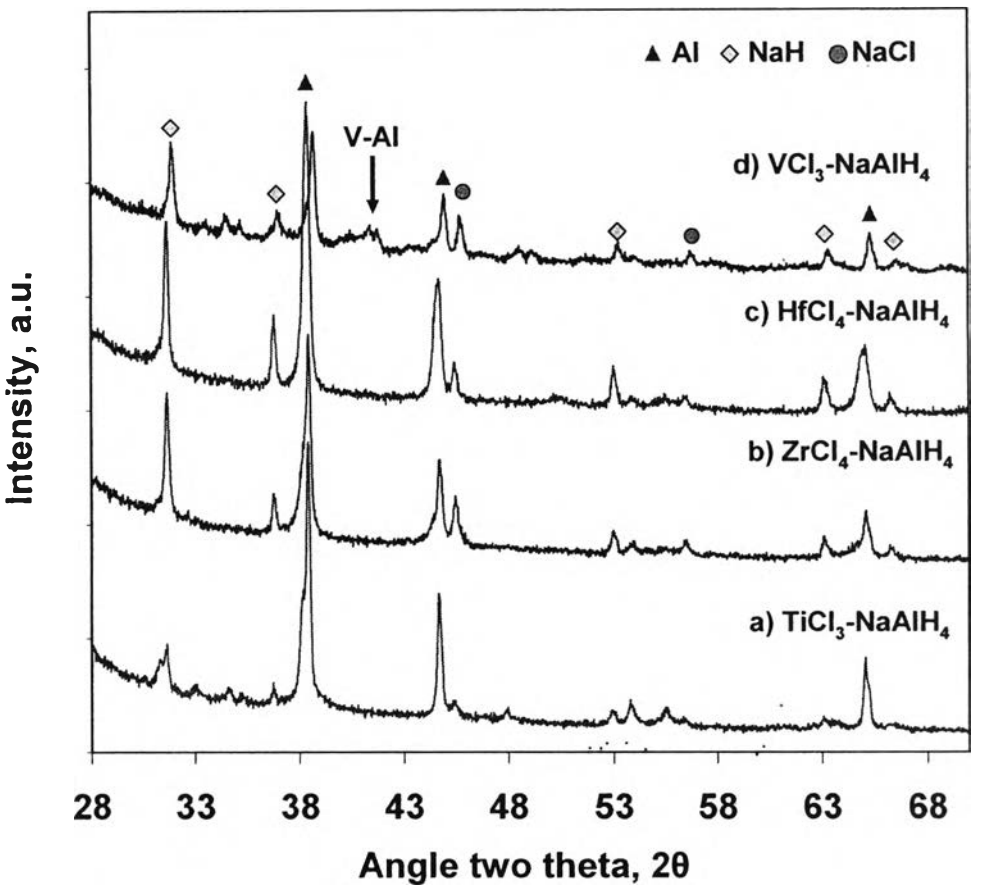

Figure 4.12 XRD patterns of a) $TiCl_3$-$NaAlH_4$, b) $ZrCl_4$-$NaAlH_4$, c) $HfCl_4$-$NaAlH_4$, and d) VCl_3-$NaAlH_4$ after hydrogen desorption.

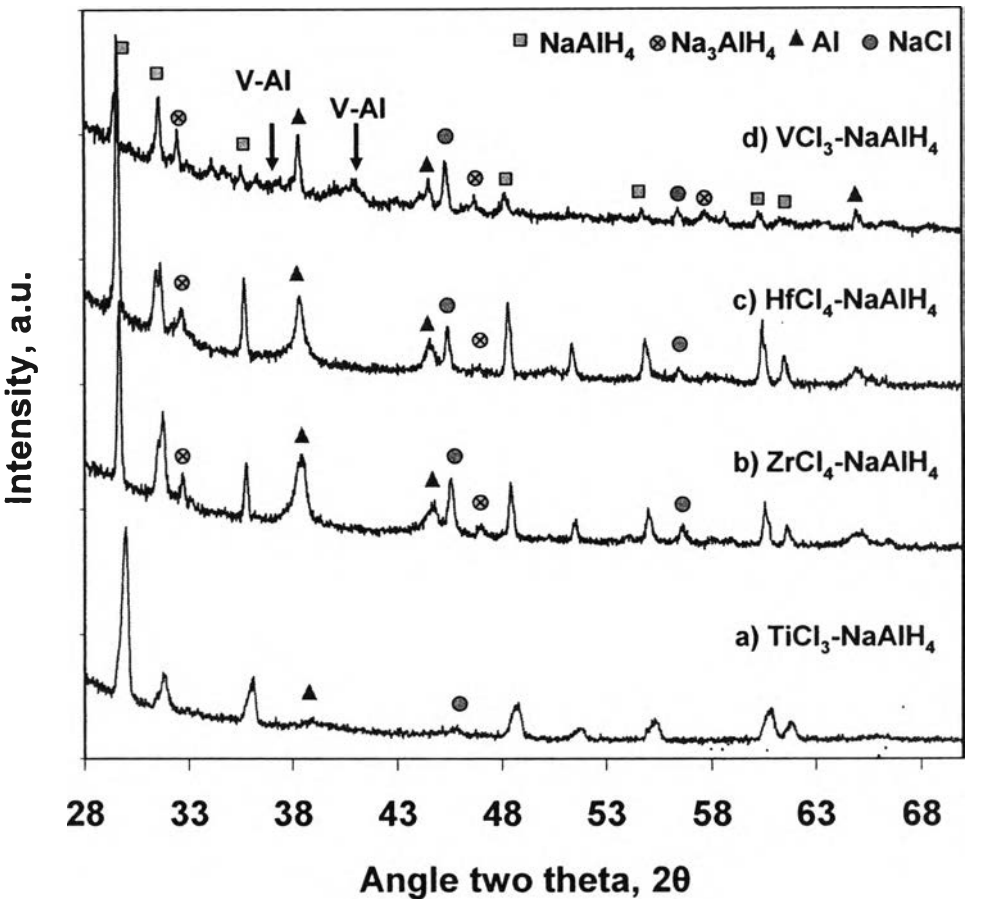

Figure 4.13 XRD patterns of a) $TiCl_3$-$NaAlH_4$, b) $ZrCl_4$-$NaAlH_4$, c) $HfCl_4$-$NaAlH_4$, and d) VCl_3-$NaAlH_4$ after hydrogen re-absorption.

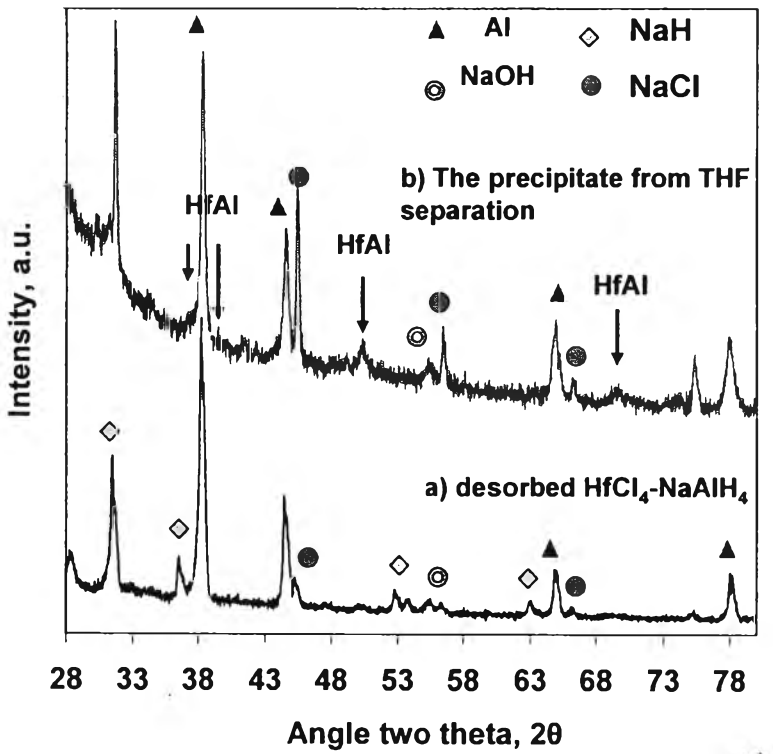

Figure 4.14 XRD patterns of a) desorbed 10%$HfCl_4$-$NaAlH_4$ and b) the precipitate from THF solution.